

## Investigation of the seismic performance of precast segmental tall bridge columns

Z.Y. Bu\*<sup>1</sup>, Y. Ding<sup>1</sup>, J. Chen<sup>2</sup> and Y.S. Li<sup>1</sup>

<sup>1</sup>Faculty of Architectural, Civil Engineering and Environment, Ningbo University,  
Zhejiang Ningbo 315211, China

<sup>2</sup>Architectural Design and Research Institute of Ningbo University Co. Ltd., Zhejiang Ningbo 315211, China

(Received June 19, 2011, Revised April 6, 2012, Accepted June 1, 2012)

**Abstract.** Precast segmental bridge columns (PSBC) are alternatives for monolithic cast-in-situ concrete columns in bridge substructures, with fast construction speed and structural durability. The analytical tool for common use is demonstrated applicable for seismic performance prediction of PSBCs through experiment conducted earlier. Then the analytical program was used for parameter optimization of PSBC configurations under reversal cyclic loading. Shear strength by pushover analysis was compared with theoretical prediction. Moreover, seismic response of PSBC with energy dissipation (ED) bars was compared with its no ED bar counterpart under three history ground acceleration records. The investigation shows that appropriate ED bar and post-tensioned tendon arrangement is important for higher lateral bearing capacity and good ductility performance of PSBCs.

**Keywords:** bridge construction; concrete precast; pier; shear strength; seismic response; hollow sections; finite element method

---

### 1. Introduction

The precast segmental bridge columns (PSBC) were first used in the highway bridges of Texas State of the United States in the 1970s with the design and construction of precast girders (Billington 1999). The precast of structural components is a special construction method. Most components can be fabricated in factory, assembled in site, normally with post-tensioned tendons. This construction procedure can accelerate construction schedule, increase construction quality, decrease environmental impact in construction site, and mitigate traffic congestion and vehicle carbon dioxide emission in urban areas (Ou 2010a).

In seismic design of bridge structures, as the development of capacity-based design, modal pushover analysis is preferable in determining capacity curve (Kwak 2009). But for research purpose, simulation of pseudo static cyclic loading and earthquake shake table response are main concern. Many researchers have carried out experimental and analytical investigation upon the seismic performance of PSBCs (Ou 2010a, Billington 2004, Hewes 2002, Chou 2006, Wang *et al.* 2008b). The PSBC has large displacement ductility, strong self-centering ability, and normally less

---

\*Corresponding author, Lecturer, E-mail: [buzhanyu@yahoo.com.cn](mailto:buzhanyu@yahoo.com.cn); [buzhanyu@nbu.edu.cn](mailto:buzhanyu@nbu.edu.cn)

opportunity be damaged during earthquake. But this structural system also has unsolved deficiencies, such as low energy dissipation capacity and 20 to 30 percent larger displacement demand compared with the monolithic cast-in-situ columns (Kwan 2003). To overcome these imperfections of PSBC, many researchers have proposed improved schemes of PSBC, such as energy dissipation bars scheme by Ou (2010a, b) and Wang (2008a), the concrete filled steel tube with energy dissipater scheme by Chou (2008), the steel tube shear connectors scheme by Shim (2008), Kim (2010), and the hybrid connection system by Palermo (2007). The stress concentration and discontinuous deformation may exist in longitudinal reinforcing bars at the location of column-foundation interface due to anchorage slip, shear slip and penetration (Kim 2008), which will lead to premature fracture of reinforcing bars. Ou (2010a) proposed setting certain unbonded length in reinforcing bars at the location of base joint to mitigate the stress concentration and premature fracture phenomena.

Despite the plenty of test validation on the superior performance of PSBCs under monotonic and reversal cyclic loading, shear strength prediction and simulation of earthquake response on these systems is lacking. Work is underway by the first author cooperate with the State Key Laboratory of Bridge Engineering Structural Dynamics to investigate the seismic performance of PSBCs of cross sea bridge on three dimensional shake table. The loading history of PSBC under reversal cyclic or monotonic tip displacement mainly includes three stages, decompression of base joint, before elongation of prestressing tendon, after elongation of prestressing tendon (Hewes 2002).

This paper provided analytical simulation of earthquake response of PSBCs. First the PSBC was modeled with fibre beam-column element method. Then the model was verified though reversal cyclic load test data. Subsequently, the model was used to carry out parametric study to help improve the design of PSBCs. Shear strength prediction was given special emphasis. A three-dimensional (3D) finite element (FE) model was also established to compare with the fibre beam-column element model. At last a suite of earthquake records were applied to typical PSBCs to investigate the effect of ED bar in controlling seismic response.

## 2. Pseudo static test of precast segmental tall bridge column

The precast segmental tall bridge column reversal cyclic test specimen P3 conducted in Taiwan University were taken as object of investigation (Wang 2008a). The specimens were composed of rectangular hollow column, top rectangular solid load stub and foundation. The prototype column was 50 meter high, considering a scale ratio of 0.4, assuming the column with two reversed bending points, half column height of about 10 meter was used in experiment and simulation. The post-tensioned force and the superstructure axial load were both 4000 kN. The transverse stirrups utilized  $\phi 13$  reinforcement bars. The longitudinal reinforcement within the segment used  $\phi 22$  reinforcement bars. The energy dissipation reinforcement through the segmental joints used  $\phi 36$  high performance bars. The post-tensioned tendon utilized seven wire steel strand with a nominal diameter of 12.7 mm. The material property is listed in Table 1. The post-tensioned tendons were distributed through the whole length of the column, while ED bars were arranged in footing and S1 to S5 segments. The specimen P3 is the main object for investigation, so its configuration is given special attention. A total of 20 ED bars were placed in segment S1. And 12 ED bars were laid in segment S2 to S3, 8 ED bars in segment S4 to S5. The post-tensioned tendon ratio is 0.41%. The ED bar ratio of segment S1 is 1.41%, while for segment S2 to S3 is 0.85%, for segment S4 to S5 is 0.57%. The

Table 1 Material property

Concrete compression strength	Grout compression strength	Energy dissipation bar		Prestressing tendon		Transverse stirrup	
		Yield strength	Ultimate strength	Yield strength	Ultimate strength	Yield strength	Ultimate strength
44	36	490	686	1792	1888	511	681

Note: All strength units expressed in MPa.

superstructure gravity load was imposed through reaction frame at column tip using four hydraulic jacks stretching four threaded rods which were connected to the strong floor. The test was displacement controlled. The relative displacement of top displacement to lateral force act point height  $H$  (9500 mm) of each cycle was increased gradually, such as 0.25%, 0.375%, 0.5%, 0.75%, 1.0%, 1.5%, 2.0%, 3.0%, 4.0% and 5.0%, each cycle repeated twice.

### 3. Finite element model

A nonlinear structural analysis program, Open System for Earthquake Engineering Simulation (OPENSEES), was used for the seismic analysis of PSBCs. The program was developed by the Pacific Earthquake Engineering Research Center of University of California Berkeley. It was an open source and object oriented program, the program and source files can be download from its homepage <http://opensees.berkeley.edu/>.

The column section is divided into a number of fibres, assuming plane sections remain plane and normal to the longitudinal axis. The concrete cracking and reinforcement rebar bond-slip effects are overlooked in element. The concrete cracking effect is only significant in the pre-yield phase of response and can be neglected in studies which focus on the hysteretic behavior under large inelastic deformation reversals. Bond-slip deformation is challenging problem to be considered in beam element section, which is beyond the scope of the present study. Shear effect is not considered in the element in that it has little influence on the lateral strength of the large span to depth ratio column. The section was divided into fibres to simulate the changes of concrete and steel reinforcement area along the element length. Section stiffness and resisting force can be determined through integration of the corresponding fibre stress. The element equilibrium equation is formed by force and displacement mixed method (Spacone 1996), which gives fine solution than the conventional force based method.

#### 3.1 Fibre finite element model

The finite element model of the precast segmental bridge column is built with fibre beam-column element, which has few freedoms and relatively high precision (Zhu 2006). The configuration of specimen P3 by Wang (2008a) is illustrated in Fig. 1. The column reinforcement bars are composed with bonded post-tensioned tendons, bonded energy dissipation bars, longitudinal reinforcement bars and stirrups inside segment *et al.* The column section is divided into a number of concrete fibres. The bonded post-tensioned tendons and bonded energy dissipation bars are modeled with steel fibres. The lateral reinforcement and longitudinal reinforcement inside the segment were not

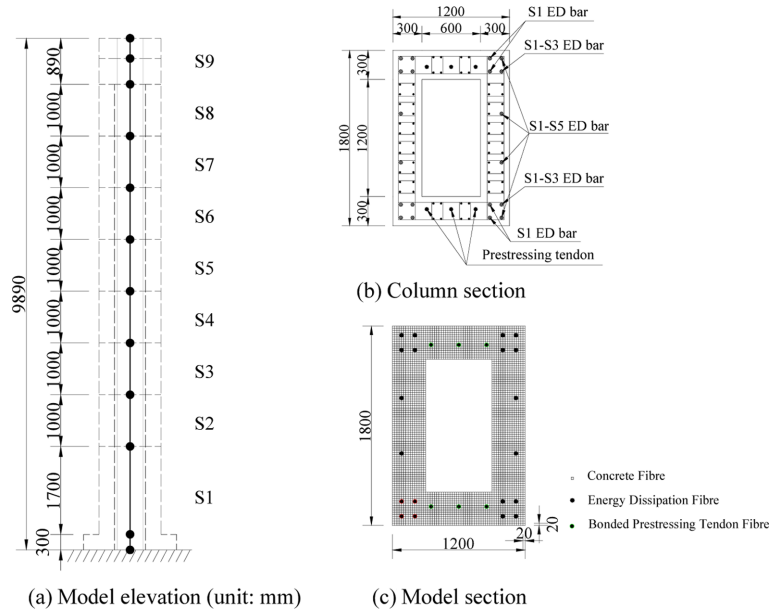


Fig. 1 Precast segmental bridge column of specimen P3

explicitly modeled. The effect was considered by using confined concrete stress-strain constitutive equation. The initial tension stress of post-tensioned tendons is modeled with initial strain. The unbonded post-tensioned tendons in the assumed specimen are modeled using truss elements with one end connecting stiff beam at column tip and the other end fixed at foundation bottom.

### 3.2 Material model

The concrete material utilized the Kent-Scott-Park model with loading and unloading stiffness degradation, which had simple form and high calculation efficiency. This model was first proposed by Park and Kent (1972), and was later revised by Scott (1982). The stress and strain relation was comprised by three parts, parabolic ascending part, linear descending part and the horizontal part. The tension strength was assumed to be zero which can simulate the opening of joint and give small error to segment concrete response. Fig. 2(a) shows a typical hysteretic stress-strain curve of concrete.

The energy dissipation bars used the Giuffre-Menegotto-Pinto material model (Menegotto 1973). In this steel model, linear distribution of strain along the depth of section was assumed (plane section remain plane assumption), excluding bond slip during all the loading history, and local buckling of steel bars. The properties of the materials were assumed not to deteriorate after repeated stressing, while Bauschinger effect on steel was considered. Fig. 2(b) shows a typical hysteretic stress-strain curve of steel reinforcement.

The post-tensioned tendon was assumed to conform bilinear elastic-plastic material model, the second stiffness was properly chosen referring Hewes (2002).

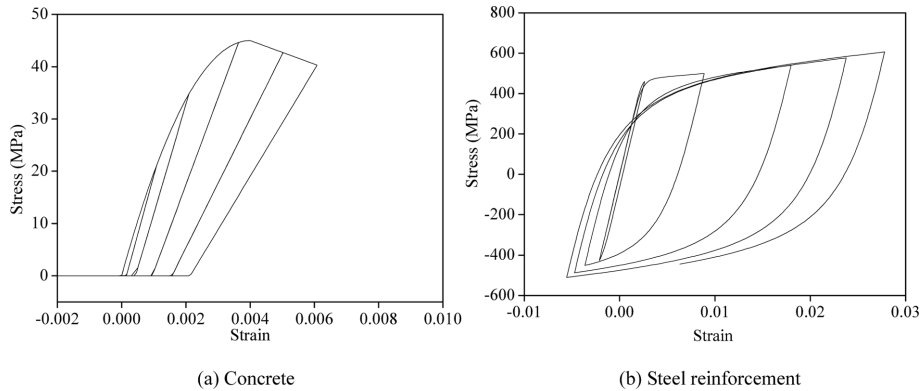


Fig. 2 Typical stress-strain hysteretic curves

#### 4. Model validation

The comparison of load-displacement hysteretic curve by fibre beam-column element simulation and experiment was shown in Fig. 3. The load-displacement hysteretic curve of specimen P3 in experiment had a sudden drop of bearing capacity at the maximum displacement because of reinforcement bar fracture. The specimen P3 joint opening between segment S1 and S2 by simulation was about 42 mm, close to the experiment result 45 mm. Fig. 3 indicates that the force-displacement response by the fibre model analyses generally agree well with the experimental data.

The specimen P3 moment-curvature relation was calculated by the analytical method in the component level and by UC-Fiber program in the section level respectively. The calculation results of moment-curvature were shown in Fig. 4. The analytical method uses the definition of curvature  $\phi$  of plastic hinge by Eq. (10) in the fibre beam-column element model. Select a node near center of plastic hinge length  $L_p$  defined by Eq. (9). Output the concrete strain  $\varepsilon_c$  and  $\varepsilon_t$  at compression and tension edge from the analytical model at various tip displacement level. Then from the linear distribution assumption of strain along the section height, one can easily get the section compression height  $c = \varepsilon_c \cdot h / (\varepsilon_c - \varepsilon_t)$ , where  $h$  is section depth. Then the curvature can be written as  $\phi = \varepsilon_c / c = (\varepsilon_c - \varepsilon_t) / h$ . The moment  $M$  can be expressed as  $M = Q \cdot L$ , where  $Q$  is base shear force,  $L$  is column height. The concrete material used Mander's confined and unconfined model, and steel reinforcement and tendon used Menegotto-Pinto model in UC-Fiber. The moment-curvature relation

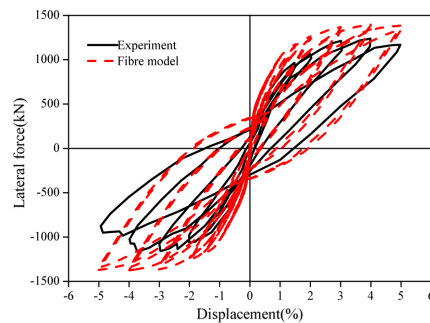


Fig. 3 Fibre model simulation and experimental data of specimen P3

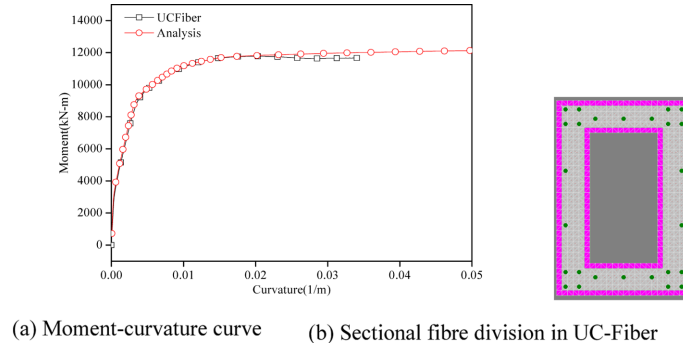


Fig. 4 Sectional moment-curvature analyses

derived by the two methods showed good agreement. The fibre beam-column model can catch main mechanical features of PSBCs, thus the model can be applied to design and optimization of PSBCs.

## 5. Parametric analysis

The applicability of OPENSEES program for PSBCs was examined through experimental database. Then the program can be used to design of PSBCs. The design parameters for precast segmental bridge columns mainly include sectional shape, segmental length, reinforcement arrangement, initial stress of tendon, axial force, column length and the post-tensioned tendon bond condition et al. The sectional shape and segmental length is not the main focus of this paper. The energy dissipation bar ratio, post-tensioned tendon ratio, the controlling tendon stress, dead load axial ratio, shear span ratio and the tendon bond condition were main concern. The influence of above parameters on the load-displacement curve and energy dissipation were investigated in this paper. All assumed specimens were based on specimen P3 by Wang (2008a). One parameter was changed each time, while the other parameters were identical with specimen P3. A total number of 18 specimens were assumed. The specimen parameters were listed in Table 2. Series A specimens have varying ED bar ratio. Series B specimens have altering tendon ratio. Series C specimens have changing tendon controlling stress. Series D specimens have variable superstructure axial loads. Series E specimens have different shear span ratio. Series F specimens have differing post-tensioned tendon bond conditions. As depicted in Table 2, it is evident that specimen A1, B2, C2, D1, E1 and F1 have the same parameters with test specimen P3.

### 5.1 Energy dissipation bar ratio

The series A specimens have variable ED bar ratio. The distribution of ED bar was the same with test specimen P3 as shown in Fig. 1(b). There are 8 ED bars ended at S1-S2 joint, which is designated as S1 ED bar. There are 4 ED bars ended at S3-S4 joint, which is designated as S1-S3 ED bar. There are 8 ED bars ended at S5-S6 joint, which is designated as S1-S5 ED bar. More details about the ED bar distribution can refer to Wang (2008a). The column sectional ED bar ratio was changed by varying the ED bar diameter. The specimen A1 has 20 ED bars of 36 mm diameter at base section corresponding to the sectional reinforcement ratio of 1.41%. The diameter of ED

Table 2 Specimens and parameters

Specimen No.	ED bar ratio (%)	Tendon ratio (%)	Tendon tension stress (MPa)	Dead load ratio (%)	Shear span ratio (%)	Tendon bond condition
P3	1.41	0.41	680	6.3	7.9	Bonded
<b>A1</b>	<b>1.41</b>	<b>0.41</b>	<b>680</b>	<b>6.3</b>	<b>7.9</b>	<b>Bonded</b>
A2	0.86	0.41	680	6.3	7.9	Bonded
A3	0.44	0.41	680	6.3	7.9	Bonded
A4	0.00	0.41	680	6.3	7.9	Bonded
B1	1.41	0.54	680	6.3	7.9	Bonded
<b>B2</b>	<b>1.41</b>	<b>0.41</b>	<b>680</b>	<b>6.3</b>	<b>7.9</b>	<b>Bonded</b>
B3	1.41	0.27	680	6.3	7.9	Bonded
B4	1.41	0.14	680	6.3	7.9	Bonded
C1	1.41	0.41	450	6.3	7.9	Bonded
<b>C2</b>	<b>1.41</b>	<b>0.41</b>	<b>680</b>	<b>6.3</b>	<b>7.9</b>	<b>Bonded</b>
C3	1.41	0.41	910	6.3	7.9	Bonded
<b>D1</b>	<b>1.41</b>	<b>0.41</b>	<b>680</b>	<b>6.3</b>	<b>7.9</b>	<b>Bonded</b>
D2	1.41	0.41	680	12.6	7.9	Bonded
D3	1.41	0.41	680	18.9	7.9	Bonded
<b>E1</b>	<b>1.41</b>	<b>0.41</b>	<b>680</b>	<b>6.3</b>	<b>7.9</b>	<b>Bonded</b>
E2	1.41	0.41	680	6.3	5.4	Bonded
<b>F1</b>	<b>1.41</b>	<b>0.41</b>	<b>680</b>	<b>6.3</b>	<b>7.9</b>	<b>Bonded</b>
F2	1.41	0.41	680	6.3	7.9	Unbonded

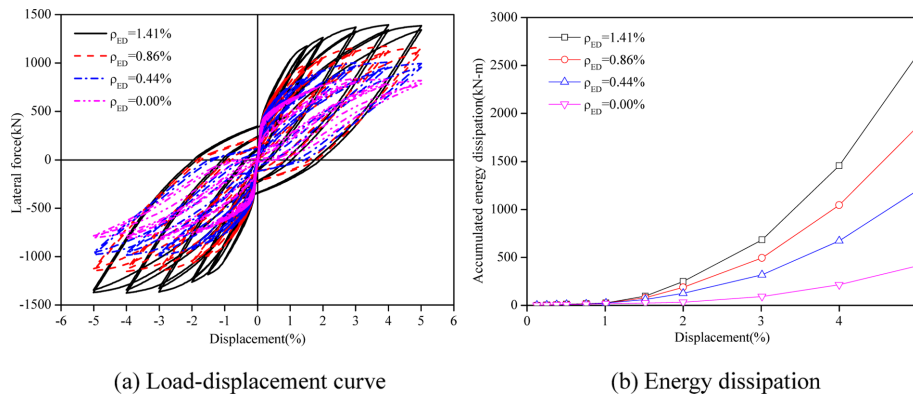


Fig. 5 Influence of ED bar ratio

bars in specimen A2 is 28 mm and sectional reinforcement ratio is 0.86%. The specimen A3 has 20 ED bars of 20 mm diameter and 0.44% reinforcement ratio. The specimen A4 has no ED bar and 0.00% reinforcement ratio. Fig. 5 shows the influence of ED bar ratio on the load-displacement curve and the energy dissipation of PSBC. With the increasing of ED bar ratio, the column lateral bearing capacity was enhanced. When the displacement first reached 5%, from specimen A4 to A1,

the lateral bearing capacity was 819 kN, 995 kN, 1162 kN and 1386 kN respectively. The residual displacement was increased with the increasing of ED bar ratio. With the increasing of ED bar ratio, the energy dissipation was also increased remarkably. Ou (2010a) proposed the increased bending moment capacity by ED bars to the moment capacity provided by column without ED bars must be less than 35% to ensure the maximum residual drift not exceed 1% before failure. Palermo (2007) also suggested the ratio between the self-centering moment contribution provided by the unbonded tendons and the dissipation moment contribution by gravity axial load be restricted between 1.15-1.25 in order to provide sufficient dissipation capacity to limit maximum displacements and maintain full re-centering. Appropriate ED bar ratio for necessary bending moment capacity and less residual displacement needs more experimental investigation.

### 5.2 Post-tensioned tendon ratio

The post-tensioned tendons are all distributed through the entire height of column, and are anchored at foundation bottom and column tip. The post-tensioned tendon ratio can be changed through varying the bundle numbers of tendon. Specimen B1 has 8 bundles of 7 wire  $\phi 5$  strands, with a post-tensioned tendon area of 7840 mm<sup>2</sup>, and the corresponding tendon ratio (ratio of tendon area to total section area) is 0.54%. Four bundles of strands were evenly placed on one web symmetric about the sectional center in length of 600 mm. Specimen B2 has 6 bundles of 7 wire  $\phi 5$  strands, with a post-tensioned tendon area of 5880 mm<sup>2</sup>, and the corresponding tendon ratio is 0.41%. The space between strand bundles is 250 mm, as shown in Fig. 1(b). Specimen B3 has 4 bundles of 7 wire  $\phi 5$  strands, with a post-tensioned tendon area of 3920 mm<sup>2</sup>, and the corresponding tendon ratio is 0.27%. The space between strand bundles is 200 mm. Specimen B4 has 2 bundles of 7 wire  $\phi 5$  strands, with a post-tensioned tendon area of 1960 mm<sup>2</sup>, and the corresponding tendon ratio is 0.14%. The strand bundles are center placed on two webs. The influence of post-tensioned tendon ratio on the load-displacement curve and energy dissipation was illustrated in Fig. 6. With the increasing of post-tensioned tendon ratio, lateral bearing capacity increased. From B4 to B1, the lateral bearing capacity was 1048 kN, 1229 kN, 1386 kN and 1537 kN respectively. With increasing of tendon ratio, the column energy dissipation increased. From B4 to B1, the accumulated energy dissipation was 2284 kN-m, 2418 kN-m, 2620 kN-m and 2749 kN-m separately, but the incremental amplitude is not prominent.

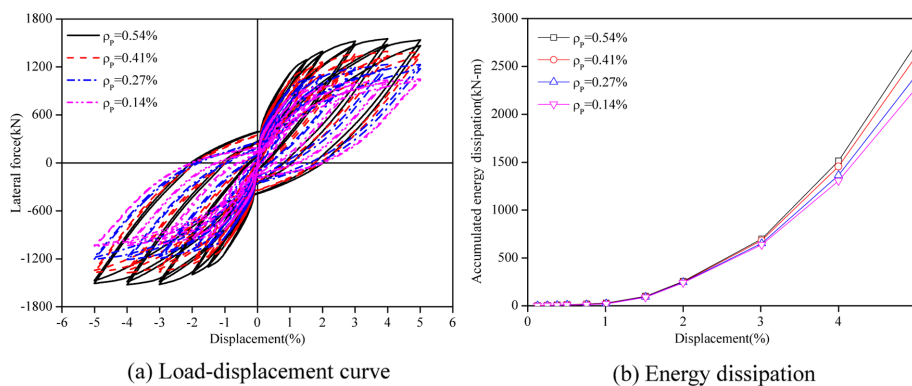


Fig. 6 Influence of tendon ratio

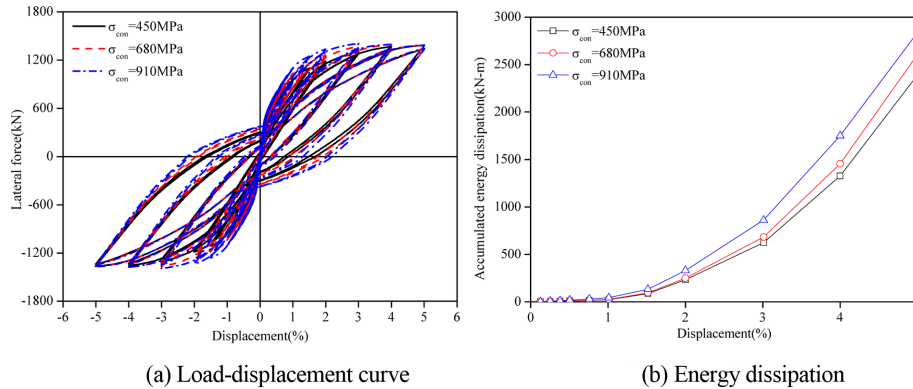


Fig. 7 Influence of tendon controlling tension stress

### 5.3 Post-tensioned tendon controlling tension stress

The post-tensioned tendon amount remains 6 bundles of 7 wire  $\phi 5$  strand, the load-displacement curve and energy dissipation variation with the varying tensioning stress is investigated. The total tendon tensioning force of specimen C1 is 2646 kN, corresponding to the controlling tension stress of 450 MPa. For specimen C2 the total tensioning force is 4000 kN, and the controlling tension stress is 680 MPa. The total tensioning force of specimen C3 is 5351 kN, corresponding to controlling tension stress of 910 MPa. The interaction of controlling tendon tension stress upon the response of pseudo static cycle loading is illustrated in Fig. 7. The lateral bearing capacity is not sensitive to the tension stress of strands. From specimen C1 to C3, the lateral bearing capacity was 1384 kN, 1386 kN and 1387 kN respectively at 5% drift. Residual displacement slightly increases with increasing of tendon controlling stress from 450 MPa to 910 MPa. This may be caused by unloading from post-yield stage of tendon. In structural design practice, tendon controlling stress can be carefully chosen to ensure that the tendon stress at maximum design displacement is less than yield stress to avoid unloading residual displacement. The energy dissipation has a slightly increase with the raising of controlling tension stress. For specimen C1 to C3, the accumulated energy dissipation was 2402 kN-m, 2620 kN-m and 2852 kN-m respectively.

### 5.4 Superstructure axial load compression ratio

The superstructure axial load of P3 column is 4000 kN, which is the case for specimen D1. The dead load axial ratio is  $N/f_c'A = 4000 \times 1000/44/1440000 = 6.3\%$ . The superstructure axial load of specimen D2 is 8000 kN, corresponding to an axial compression ratio of 12.6%. For specimen D3 the superstructure dead load is 12000 kN, which has an axial compression ratio of 18.9%. The analytical results are shown in Fig. 8. The column lateral bearing capacity is increased with the augment of axial compression ratio. From column D1 to D3, the lateral bearing capacity is 1386 kN, 1570 kN and 1721 kN respectively. The residual displacement is reduced slightly with enhancement of axial compression ratio. The energy dissipation is increased weakly with augment of axial compression ratio, from specimen D1 to D3 the energy dissipation is 2620 kN-m, 2868 kN-m and 3048 kN-m respectively.

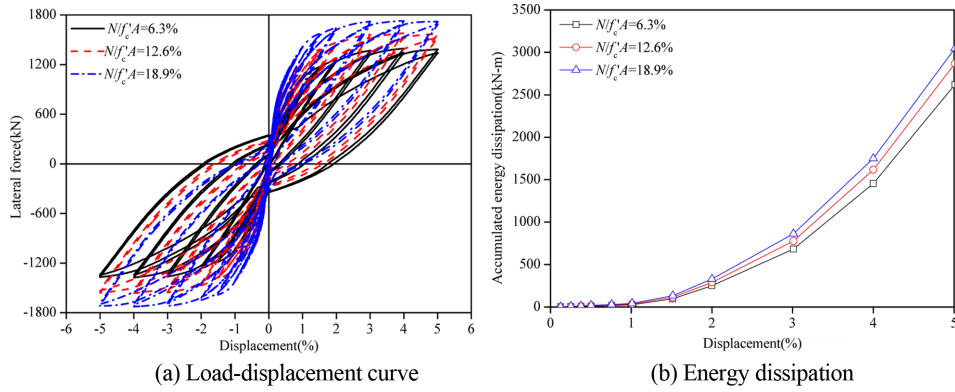


Fig. 8 Influence of superstructure axial load compression ratio

### 5.5 Shear span ratio

The test specimen P3 with a height of 9500 mm is designated as specimen E1, whose shear span is  $M/D = H/D = 9500/1200 = 7.9$ , where  $M$  is bending moment,  $V$  is section shear force,  $D$  is section depth. Another column E2 is assumed only containing segment S1 to S5, with a height of 6500 mm, and the corresponding shear span ratio is  $H/D = 6500/1200 = 5.4$ . The ED bar layout of specimen E2 is the same with test specimen P3. The prestressing tendon is distributed at the same location of section and full length of column height, but the length is shortened with shortening of column height. The influence of shear span on the load-displacement curve and energy dissipation is depicted in Fig. 9. The lateral bearing capacity is enhanced with decreasing of shear span ratio. The lateral bearing capacity for short column E2 is 2141 kN, while for high column E1 is 1386 kN both at 5% drift. The residual displacement is increased significantly with the reduction of shear span ratio. The energy dissipation has minimal increase with column becoming shorter both at 5% drift due to increasing of lateral bearing capacity in short column.

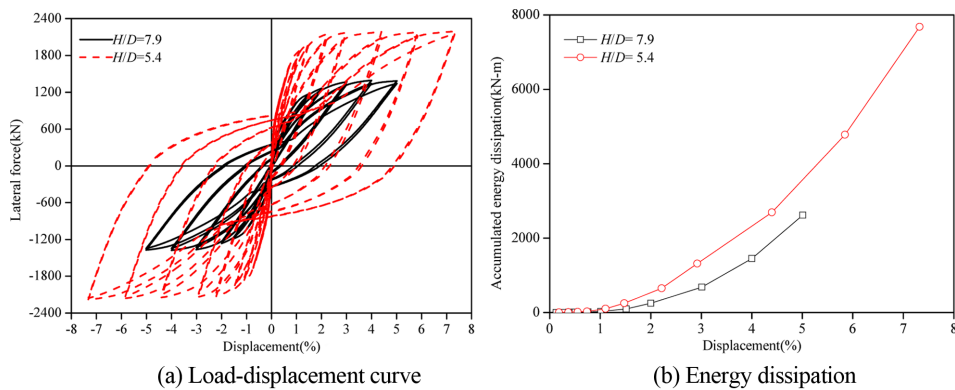


Fig. 9 Influence of shear span ratio

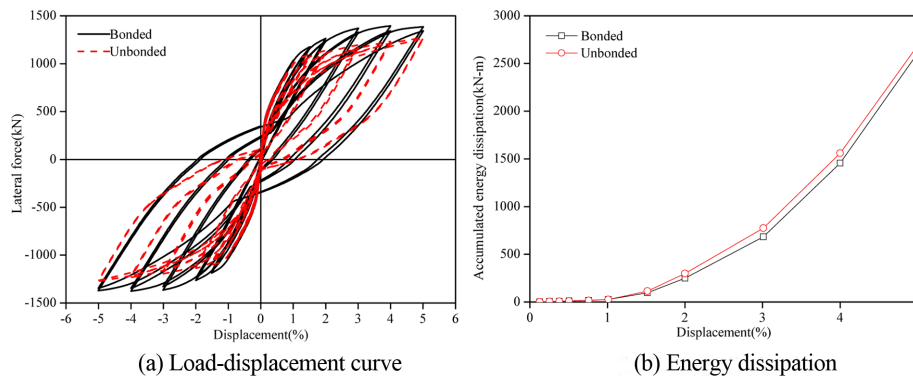


Fig. 10 Influence of tendon bond condition

### 5.6 Tendon bond condition

The test specimen P3 utilizes bonded post-tensioned tendon, which is designated as column F1. The corresponding unbonded case is designated as column F2. The six unbonded post-tensioned tendons are modeled with three truss elements. One truss element represents a pair of tendons at the same location in loading plane. One end the truss element is anchored in foundation, and the other end is anchored onto rigid beam in column tip. The initial tension force is simulated with initial strain. The analytical results are shown in Fig. 10. The bonded post-tensioned tendon provides higher lateral bearing capacity, which is 1386 kN at 5% drift, and it is only 1272 kN for the unbonded case. The residual displacement of the bonded column F1 is much larger than the unbonded column F2. The energy dissipation for the bonded tendon column is a little lower than the unbonded case. In the bonded tendon column, the reloading stiffness deterioration occurs due to large residual displacement. But for the case of unbonded column, the residual displacement is neglectable, and the reloading stiffness degradation is small. So although the lateral capacity of bonded column is higher than the unbonded case, the energy dissipation (area enclosed by force-displacement curve) is relatively small. In column seismic design, lateral bearing capacity is normally not the controlling factor, so the unbonded tendon is more preferable for its high energy dissipation and low residual displacement which requires less post quake retrofit.

### 5.7 Shear strength

Seismic design based on capacity protection requires preventing brittle failure of bridge structures. The bridge structures were expected to behave in ductile manor under seismic excitation. The brittle failure such as shear or flexural shear which happens abruptly is prohibited. In order to investigate shear related column behavior under seismic loads, shear strength of six precast segmental bridge column test or analytical specimens is compared with the theoretical shear strength by specifications or guidelines.

Considering the shear effect is not involved in fibre beam column element method, which may cause error for low aspect ratio columns. A three dimensional (3D) finite element (FE) model of precast segmental bridge column of specimen P3 was established with ABAQUS software. Fig. 11 shows the finite model of segmental column. The foundation and column segments were modeled

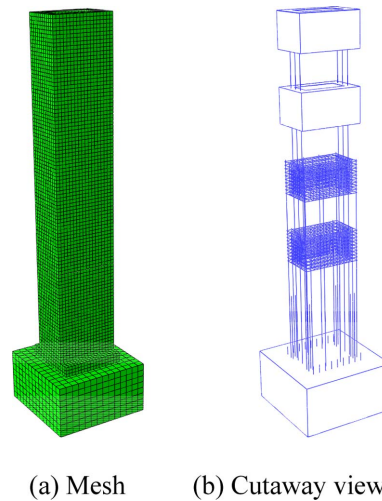


Fig. 11 3D FE model for segmental column

using eight-node solid element with reduced integration. The concrete material was modeled with concrete damaged plasticity model of ABAQUS. The steel reinforcement of stirrups and longitudinal rebar within segment was modeled with truss element and forming a steel cage embedded in concrete solid. The strain-stress behavior of steel rebar cage was bilinear model. The bonded posttensioned tendons were modeled with truss element. The initial stress was considered. The bond effect was simulated with embedded interaction. A bilinear material model was used for posttensioned tendon. ED bars was also modeled with truss element. The ED bars used similar steel material model as the rebar cage. Segment to segment or segment to foundation interaction used surface-to-surface contact element. A tangent friction coefficient of 0.8 was assumed. The normal interface behavior used hard contact. The analysis was divided into three steps. The prestressing force was act on column at first step. Then superstructure axial load was loaded on column top at second step. At last step, displacement was applied to column tip. Geometry nonlinearity is involved to account for  $P-\Delta$  effect.

The lateral load-displacement curve of the 3D FE model is depicted in Fig. 12 in comparison with experiment results of specimen P3 by Wang (2008a). The lateral shear force at foundation base at 5% drift by 3D FE model simulation is 1162 kN, which is nearly the same with experiment results of 1169 kN. But the maximum lateral bearing capacity of simulation (1162 kN) is slightly lower than experiment (1238 kN) due to material data difference with actual specimen. Unloading residual displacement by 3D FE model is much higher than experiment caused by inelastic deformation and contact slip. But the focus of this study is about the lateral bearing capacity. From Fig. 3(b) and Fig. 12, it can be concluded that the fibre beam column element is applicable to lateral bearing capacity analysis of segment columns to substitute the time-consuming 3D FE model simulation with acceptable calculation accuracy.

The concrete compression and tension stress and joint contact opening at 5% drift by 3D FE model were illustrated in Fig. 13 with a deformation scale factor 3.5. The maximum compression stress of concrete occurred at S1-S2 interface at quantity of 62 MPa. The maximum tension stress occurred at tension side in large range at quantity of 5 MPa. The maximum joint opening happened at S1-S2 joint with a value of 24 mm, which is smaller than experimental data of 45 mm. The

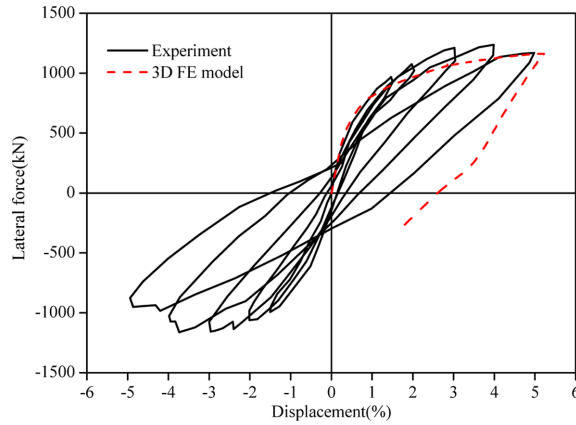
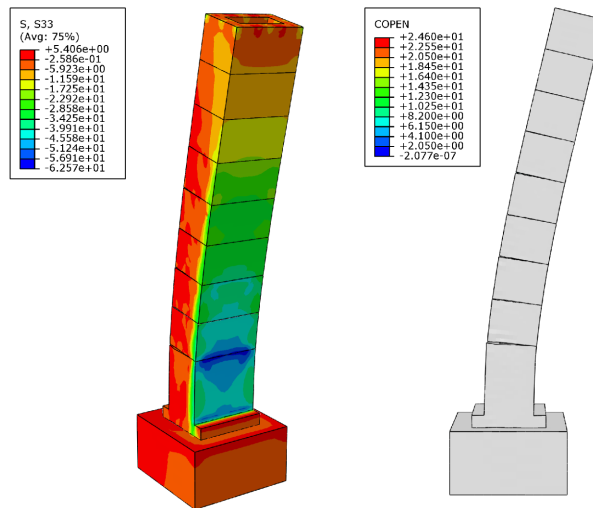


Fig. 12 Force-displacement curve of column P3 by 3D FE model and experiment



(a) Concrete vertical stress (MPa) (b) Joint opening (mm)

Fig. 13 Simulation results of column P3 with 3D FE model at 5% drift

foundation-S1 joint didn't open due to anchorage effect of d32 high strength steel bolts arranged in enlarged column toe. The simulation phenomenon was in accordance with experiment although with some minor discrepancies.

The shear strength of precast segmental bridge columns under inelastic loading is dependent on several parameters: applied shear stress level, displacement ductility, axial compression level, aspect ratio, longitudinal reinforcement ratio, and transverse reinforcement ratio. The shear strength by transverse reinforcement  $V_s$  below is for rectangular sections.

**Priestley *et al.***

Priestley *et al.* (1994, 1996) proposed Eqs. (1)~(6) to calculate the nominal shear strength of reinforced concrete columns for seismic design. The concrete component  $V_c$  is calculated by Eq. (2)

to (4) for the plastic zone considering the effect of displacement ductility (Lee 2004). The contribution of transverse reinforcement to shear strength  $V_s$  is calculated by Eq. (5) based on 35 degree truss mechanism for rectangular columns. The axial-load component  $V_p$  is calculated by Eq. (6).

$$V_n = V_c + V_p + V_s \quad (1)$$

$$V_c = k\sqrt{f'_c}A_e \quad (2)$$

$$k = \begin{cases} 0.25, & \mu_\Delta \leq 2 \\ 0.25 - 0.0835(\mu_\Delta - 2), & 2 \leq \mu_\Delta \leq 4 \\ 0.083, & \mu_\Delta = 4 \\ 0.083 - 0.01025(\mu_\Delta - 4), & 4 \leq \mu_\Delta \leq 8 \\ 0.042, & \mu_\Delta \geq 8 \end{cases} \quad (3)$$

$$A_e = 0.8A_{gross} \quad (4)$$

$$V_s = \frac{A_h f_{yh} D'}{s} \cot 35^\circ \quad (5)$$

$$V_p = 0.85P \tan \alpha = 0.85P \frac{D-c}{2L} \quad (6)$$

where  $k$  = factor varying with displacement ductility  $\mu_\Delta$ ;  $A_e$  = effective area of section;  $A_{gross}$  = total area of concrete column section;  $A_h$  = area of shear reinforcement within stirrup layer distance  $s$  ( $\text{mm}^2$ );  $f_{yh}$  = specified yield strength of lateral reinforcement;  $D'$  = distance between peripheral of stirrups;  $P$  = axial load on top of column;  $D$  = the overall section depth;  $c$  = the depth of the compression zone; and  $L$  = the length of a cantilever column.

#### AASHTO shear model for column segment

The nominal shear strength of column segments was calculated using Eq. (7) based on 45 degree truss model (AASHTO Section 5.8.3.3).

$$V_n = V_c + V_s = 0.166\sqrt{f'_c}b_v d_v + \frac{A_h f_{yh} d_v}{s} \quad (7)$$

where  $b_v$  = effective web width (total width of two walls, 600 mm);  $d_v$  = effective shear depth (0.72  $h$ , 864 mm, where  $h$  is depth of the section).

#### AASHTO shear model for column segment joint

The nominal shear strength of segment joints can be computed by Eq. (8) (AASHTO Section 5.10.11.4.4).

$$V_n = [A_{ED} f_{EDy} + 0.75(P_G + P_P)] \quad (8)$$

where  $A_{ED}$  = total area of the ED bars;  $f_{EDy}$  = yield strength of the ED bars;  $P_G$  = superstructure

gravity load; and  $P_p$  = tensioning force of tendon.

The shear strength for some of the specimens in Table 2 was calculated by pushover analysis. Five types of parameter influences was considered, including ED bar ratio, tendon ratio, superstructure axial load, shear span ratio and tendon bond condition.

The displacement ductility factor  $\mu_\Delta$  can be derived from the concentrated plastic joint solution. The plastic joint length  $L_p$  can be computed by Eq. (9) (Priestley 1996).

$$L_p = 0.08L + 0.022f_{ye}d_{bl} \geq 0.044f_{ye}d_{bl} \quad (9)$$

where  $L$  = distance from the dangerous section to reversed bending point;  $f_{ye}$  = yield strength of longitudinal reinforcement; and  $d_{bl}$  = diameter of longitudinal reinforcement. The second term accounts for the additional length of plastic hinge by steel reinforcement strain penetration into the supporting elements, i.e., the foundation.

In the plastic hinge region, the column curvature  $\phi$  can be computed by Eq. (10).

$$\phi = \frac{\varepsilon_c}{c} \quad (10)$$

where  $\varepsilon_c$  = compression strain of concrete at plastic hinge region; and  $c$  = section compression region height. The yield curvature  $\phi_y$  can be derived from the linear fitting of the  $M-\phi$  curve. The yield displacement can be computed by Eq. (11). Thus the displacement ductility can be derived by Eq. (12).

$$\Delta_y = \frac{\phi_y L^2}{3} \quad (11)$$

$$\mu_\Delta = \frac{\Delta}{\Delta_y} \quad (12)$$

The shear strength calculated by pushover analysis and predicted by three shear strength models using Eqs. (1)~(12) were depicted in Fig. 14.

The shear strength of specimen A1 by pushover analysis was 1376 kN at 5% drift, which was nearly the same with pseudo static cyclic test analysis result of 1386 kN, but was bigger than the test result of 1238 kN. The shear strength by Priestley was 4334 kN at initial, and was 3089 kN at 5% drift. The shear strength by AASHTO for segment was 1743 kN, which was slightly higher than the analytical and test results. The shear strength by AASHTO for segment joint was 15949 kN, which was nearly 10 times of analytical or test results. The A1 column was finally failed in ductile flexural manner. Both Priestley *et al.* and AASHTO for segment shear strength model gave exorbitant prediction. And the applicability of AASHTO for segment joint shear strength model was doubtful, joint shear strength normally be less than segment for the discontinuous of concrete and partial longitudinal reinforcement.

The shear strength of specimen A4 by pushover was 805 kN at 5% drift, nearly the same with pseudo static cyclic loading analytical result 819 kN. The shear strength by Priestley was 4334 kN at initial, and was 2983 kN at 5% drift. The shear strength by AASHTO for segment was 1743 kN, which was nearly 2 times the analytical result. The shear strength by AASHTO for segment joint was 6000 kN, which was nearly 7 times of analytical result. This reveals one defect of Priestley and AASHTO for segment shear strength model, the longitudinal reinforcement is not considered in the

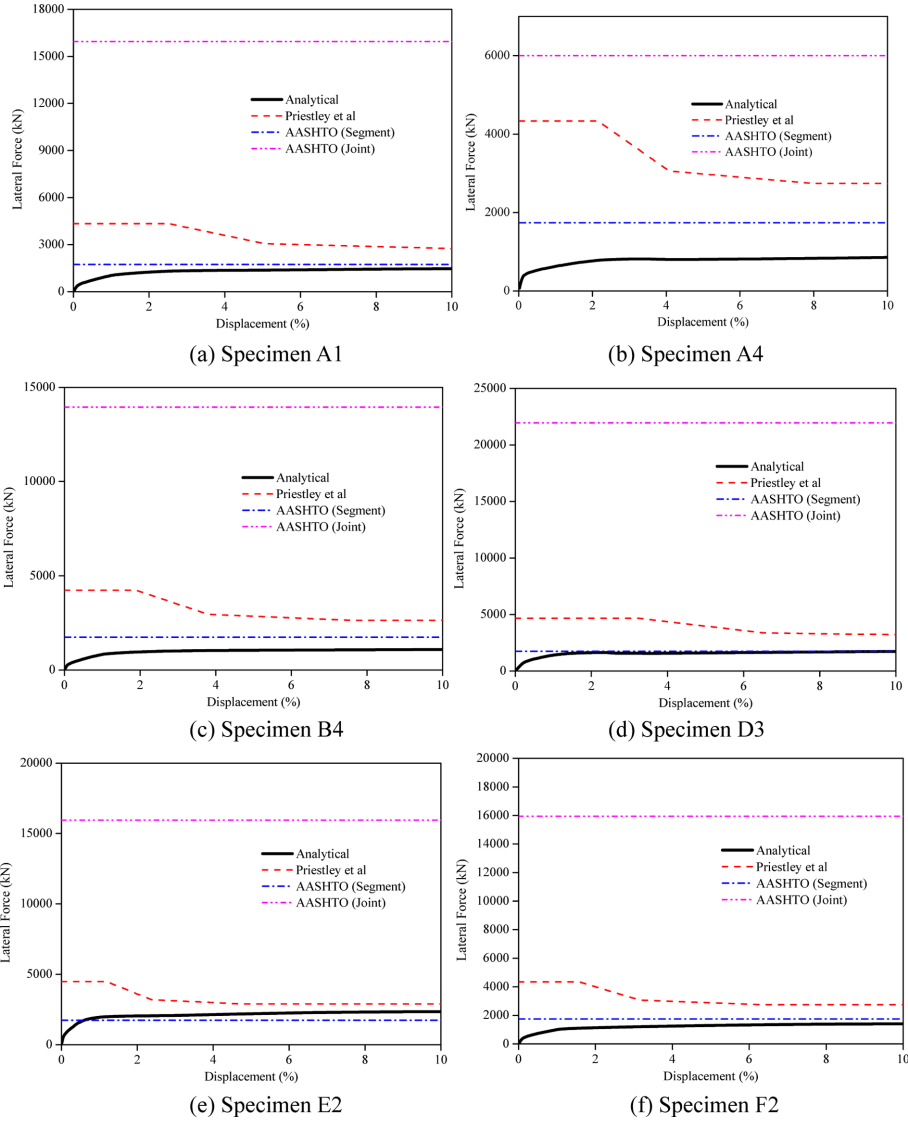


Fig. 14 Comparison of analytical and predicted shear strength

expressions, but it plays an important role in fact. In this case, no ED bar existed through segment joints, so the shear strength by specifications gave relatively higher estimation.

The shear strength of specimen B4 by pushover was 1048 kN at 5% drift, the same with cyclic loading analysis. The shear strength predicted by Priestley *et al.*, AASHTO for segment and AASHTO for joint was 2852 kN, 1743 kN and 13949 kN respectively at 5% drift. All of the three calculation models overvalued the real shear strength in case of flexural failure.

The shear strength of specimen D3 by pushover was 1599 kN at 5% drift, a little smaller than cyclic loading analysis result 1721 kN. The shear strength predicted by Priestley *et al.*, AASHTO for segment and AASHTO for joint was 3971 kN, 1743 kN and 21949 kN respectively. In which, the AASHTO for segment shear strength model provided most precise prediction. But the other two

models relatively overestimated the shear strength of column.

The shear strength of specimen E2 is underestimated by AASHTO for segment model since E2 has a relatively low aspect ratio ( $M/VD$ ) 5.4. The Priestley et al shear strength model gives better prediction. All the three shear strength models provided nonconservative prediction for specimen F2, the AASHTO for segment shear strength model provided good prediction.

From above analysis of the shear strength of segmental columns, it can be concluded: (1) Priestley *et al.* shear strength model is applicable to low aspect ratio columns, such as  $\lambda = M/VD = H/D \leq 5$ ; (2) AASHTO for segment shear strength model is appropriate for well confined, large reinforcement ratio flexural failure type column; (3) AASHTO for joint shear strength model overestimates joint shear strength, for not considering friction coefficient variation at interface with joint opening.

## 6. Seismic response

The column ultimate bearing capacity and maximum displacement under reversal cyclic loading were the main concern in pseudo static test. The response under seismic dynamic loading usually had some differences with that from pseudo static loading. So it is necessary to investigate the response of PSBCs under history ground motions. Three history ground acceleration waves from PEER strong motion database were selected as excitation, namely Loma Prieta (1989), Northridge (1994), Imperial Valley (1979), as shown in Fig. 15. The ground acceleration waves were shown in Fig. 15. The three ground acceleration waves have varying features, among which Loma Prieta had long last time and relatively concentrated energy input, Northridge was composed with short period excitation, Imperial Valley had strong intensity.

To investigate the seismic resistance of PSBCs with energy dissipation bars, specimen A1 with 1.41% energy dissipation bar ratio (Prestressed and reinforced column, abbreviated as PRC) and specimen A4 without energy dissipation bars (Prestressed column, abbreviated as PC) of Table 2

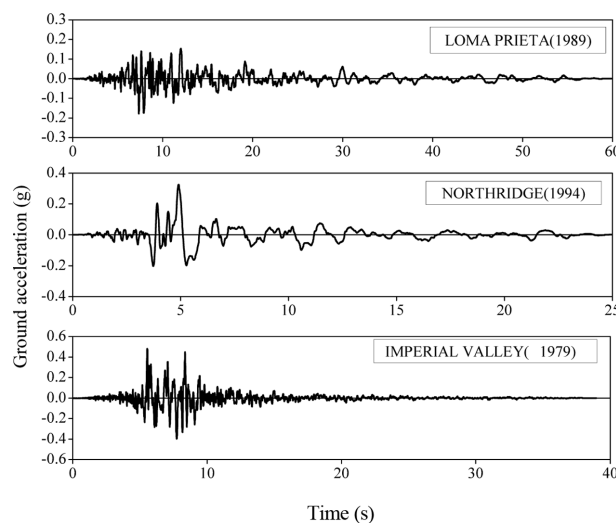


Fig. 15 Ground acceleration waves

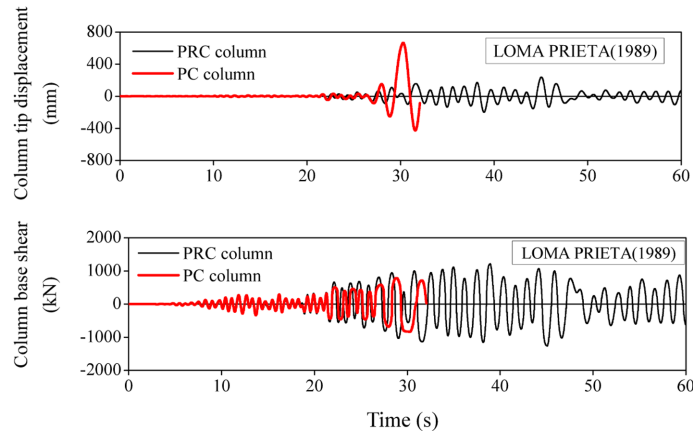


Fig. 16 Column response under Loma Prieta ground acceleration

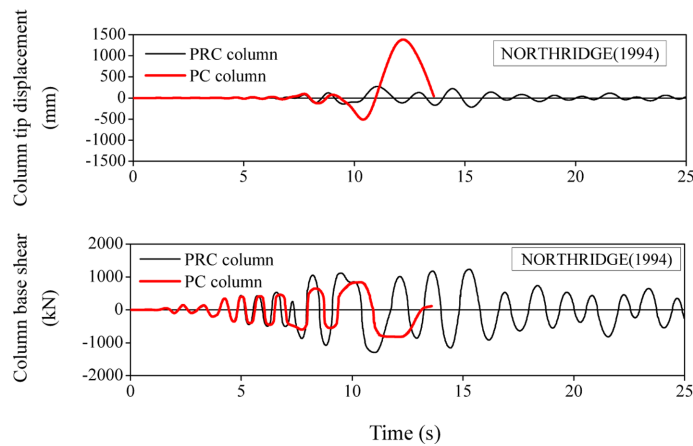


Fig. 17 Column response under Northridge ground acceleration

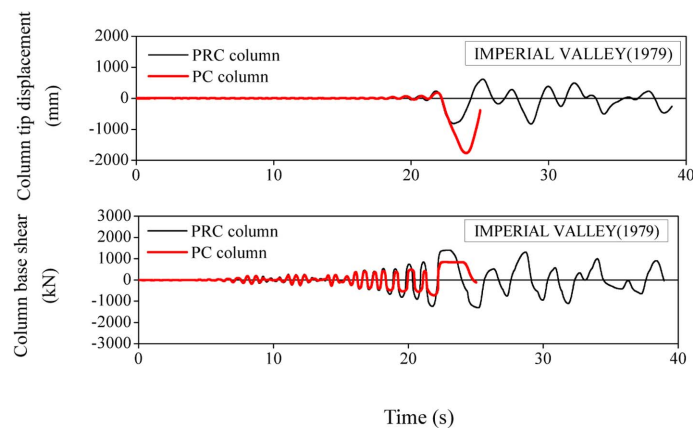


Fig. 18 Column response under Imperial Valley ground acceleration

Table 3 Seismic history response comparison of PSBC

Ground acceleration	Maximum ground acceleration (g)	Column type	Maximum base shear (kN)	Maximum tip displacement (mm)	Failure mode
LOMA PRIETA (1989)	0.1774	PRC	1261.5	238.7	N/A
		PC	834.6	665.2	Concrete crush
NORTHRIDGE (1994)	0.3254	PRC	1298.2	273.0	N/A
		PC	835.5	1383.8	Concrete crush
IMPERIAL VALLEY(1979)	0.4798	PRC	1401.4	828.1	N/A
		PC	842.1	1766.8	Concrete crush

were selected to investigate the column seismic response under the three history ground acceleration records. The column tip displacement and base shear under the three ground acceleration waves were illustrated in Fig. 16, Fig. 17 and Fig. 18. The tip displacement of PC column was larger than that of PRC column, and the PC column was ultimately damaged. But the base shear of PC column was relatively smaller than that of PRC column.

The ground acceleration and column response summary were shown in Table 3. The column tip displacement and base shear force increased with raising of ground acceleration. The column seismic response under Imperial Valley ground acceleration was analyzed for illustration. The base shear of PRC was 1401.4 kN, which is close to the pseudo analysis result of 1386 kN. The tip displacement of PRC was 828.1 mm, corresponding to relative displacement of  $828.1/9500 = 8.7\%$ , which was near limit state though not damaged. The base shear of PC was 842.1 kN, which exceeded the pseudo static result of 819 kN. The tip displacement of PC was 1766.8 mm, corresponding to the relative displacement of  $1766.8/9500 = 18.6\%$ , which was far beyond the bearing capacity of the column and lead to failure of the column in the mode of concrete crush. It can be drawn from above that column lateral bearing capacity can be enhanced by adding bonded energy dissipation bars, and the column tip displacement be restricted to relatively low level, thus the column damage be postponed.

The seismic response of PRC can be explored in frequency domain, the Fourier transformation of ground acceleration and column tip displacement were illustrated in Fig. 19. The first mode frequency of PRC was 1.31 Hz, the modal shape was vibration in longitudinal direction (about weak axis). Under the excitation of Loma Prieta ground acceleration, PRC tip displacement response showed one peak frequency, which was resonance at the natural frequency of the PRC, but slightly lower. This result may be attributed to the softening of the system, the column frequency decreased with the incurred damages. But under the excitation of Northridge ground acceleration, the PRC response showed two peak frequencies, one was the ground acceleration frequency and the other was the natural frequency of the PRC. Under the excitation of Imperial Valley ground acceleration, the PRC response also had two peak frequencies, one was the earthquake excitation, the other was the natural frequency of the PRC, but much lower due to more severe incurred damage.

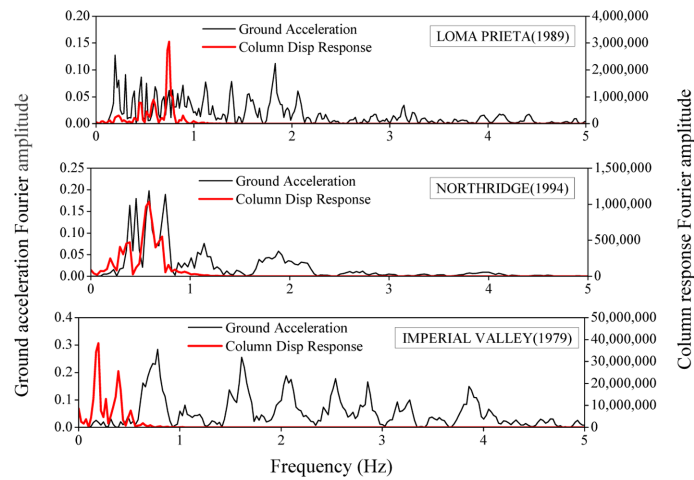


Fig. 19 Ground acceleration and PRC displacement response Fourier transformation

## 7. Conclusions

A study was carried out to investigate the seismic performance of precast segmental bridge columns (PSBC) in conjunction with cast-in-situ RC footing. A program for common use, OPENSEES, was used to model the PSBC response under pseudo static cyclic load and seismic load. The model was proved valid through earlier experimental data. The model was then used to conduct parametric analysis of PSBCs with different layouts under axial load and reversal cyclic loading. The shear strength of PSBCs with different parameters was given special attention. And a 3D FE model was built to compare with the fibre beam-column model. Finally, seismic performance of a PSBC with ED bars was compared with its no ED bar counterpart under three history ground acceleration records. The following conclusions can be drawn:

- (1) The fibre beam-column element model can be used to investigate the seismic performance of precast segmental bridge columns with acceptable precision.
- (2) Larger bonded energy dissipation bar ratio is helpful in increasing column lateral strength and energy dissipation capacity, but also leads to high residual displacement. So a reasonable ED bar ratio is controlled by acceptable residual displacement and required lateral strength.
- (3) High ratio of post-tensioned tendon can increase column lateral strength, but has little effect on the energy dissipation capacity.
- (4) Higher post-tensioned tendon controlling tension stress has little contribution to lateral strength and energy dissipation capacity. The tendon initial stress must be carefully selected to ensure the minimum stress required for anchorage safety and maximum stress at largest displacement well below yield stress to avoid unloading residual displacement.
- (5) High superstructure axial gravity load compression ratio is beneficial for higher lateral strength and hysteretic energy dissipation within some extent. But to avoid  $P-\Delta$  failure, dead load can be controlled within  $0.2f_c'A$ , and total axial load of prestressing and dead load can be restricted below  $0.3f_c'A$ .
- (6) Small shear span ratio is useful for higher lateral strength and energy dissipation ability, but also leads to high residual displacement.

- (7) Bonded tendon provided the segmental column with higher lateral strength and residual displacement, and relatively lower energy dissipation compared with the unbonded tendon case. So unbonded tendon is more preferable for excellent performance of segmental column under earthquake loading.
- (8) The 3D FE model gives better results and more information about the stress contour and contact response than fibre beam-column element model. But the 3D FE model is also more sophisticated in building and more time-consuming. So for common design purpose, the fibre model is more applicable for segmental columns with aspect ratio higher than 5, whose shear deformation can be omitted with less influence.
- (9) The AASHTO shear strength model for segment normally gives better prediction to precast segmental bridge columns. The shear strength model by Priestley et al normally provides higher estimation than actual shear capacity, and shear model for joint exhibits very high evaluated shear capacity than reality. The applicable of these shear strength model to PSBC needs more careful investigation.
- (10) The precast segmental bridge column with ED bars showed superior performance over its no ED bar counterpart, since it survived all three wide range history ground acceleration records.

## Acknowledgements

This research is sponsored by the Public Welfare Technology Application Research Project supported by Science Technology Department of Zhejiang Province, China (Project No. 2011C31G2070026); This research is also supported by the Social Development Project (2011C50017) of Science Technology Bureau of Ningbo City, China; This work is also supported by the Zhejiang Provincial Natural Science Foundation of China (Grant No. Y1110548). Their supports are gratefully acknowledged.

## References

- AASHTO (2004), *AASHTO LRFD Bridge Design Specifications*, 3rd Edition, Washington, D.C.
- Billington, S.L., Barnes, R.W. and Breen, J.E. (1999), "A precast segmental substructure system for standard bridges", *PCI J.*, **44**(4), 56-73.
- Billington, S.L. and Yoon, J.K. (2004), "Cyclic response of unbonded posttensioned precast columns with ductile fiber-reinforced concrete", *J. Bridge Eng.*, **9**(4), 353-363.
- Chou, C.C. and Chen, Y.C. (2006), "Cyclic tests of post-tensioned precast CFT segmental bridge columns with unbonded strands", *Earthq. Eng. Struct. D.*, **35**, 159-175.
- Chou, C.C. and Hsu, C.P. (2008), "Hysteretic model development and seismic response of unbonded post-tensioned precast CFT segmental bridge columns", *Earthq. Eng. Struct. D.*, **37**, 919-934.
- Hewes, J.T. and Priestley, M.J.N. (2002), "Seismic design and performance of precast concrete segmental bridge columns", Rep. No. SSRP-2001/25, Univ. of California, San Diego.
- Kim, T.H., Kim, Y.J. and Shin, H.M. (2008), "Seismic performance assessment of reinforced concrete bridge piers supported by laminated rubber bearings", *Struct. Eng. Mech.*, **29**(3), 259-278.
- Kim, T.H., Lee, H.M., Kim, Y.J. and Shin, H.M. (2010), "Performance assessment of precast concrete segmental bridge columns with a shear resistant connecting structure", *Eng. Struct.*, **32**, 1292-1303.
- Kwak, H.G. and Shin, D.K. (2009), "An improved pushover analysis procedure for multi-mode seismic performance evaluation of bridges: (1) Introduction to numerical model", *Struct. Eng. Mech.*, **33**(2), 215-238.

- Kwan, W.P. and Billington, S.L. (2003), "Unbonded posttensioned concrete bridge piers. II: Seismic Analyses", *J. Bridge Eng.*, **8**(2), 102-111.
- Lee, J.H., Ko, S.H. and Choi, J.H. (2004), "Shear strength and capacity protection of RC bridge columns", *2004 ANCER Annual Meeting: Networking of Young Earthquake Engineering Researchers and Professionals*, USA, July.
- Menegotto, M. and Pinto, P.E. (1973), "Method of analysis of cyclically loaded R.C. plane frames including changes in geometry and non-elastic behavior of elements under combined normal force and bending", *Proceedings of the IABSE Symposium on the Resistance and Ultimate Deformability of Structures Acted on by Well-Defined Repeated Loads*, Lisbon.
- Ou, Y.C., Tsai, M.S., Chang, K.C. and Lee, G.C. (2010a), "Cyclic behavior of precast segmental concrete bridge columns with high performance or conventional steel reinforcing bars as energy dissipation bars", *Earthq. Eng. Struct. D.*, **39**(11), 1181-1198.
- Ou, Y.C., Wang, P.H., Tsai, M.S., Chang, K.C. and Lee, G.C. (2010b), "Large-scale experimental study of precast segmental unbonded posttensioned concrete bridge columns for seismic regions", *J. Struct. Eng.-ASCE*, **136**(3), 255-264.
- Palermo, A., Pampanin, S. and Marriott, D. (2007), "Design, modeling, and experimental response of seismic resistant bridge piers with posttensioned dissipating connections", *J. Struct. Eng.-ASCE*, **133**(11), 1648-1661.
- Park, R., Kent, D.C. and Sampton, R.A. (1972), "Reinforced concrete members with cyclic loading", *J. Struct. Div.-ASCE*, **98**(7), 1341-1360.
- Priestley, M.J.N., Verma, R. and Xiao, Y. (1994), "Seismic shear strength of reinforced concrete columns", *J. Struct. Eng.-ASCE*, **120**(8), 2310-2329.
- Priestley, M.J.N., Seible, F. and Calvi, G.M. (1996), *Seismic Design and Retrofit of Bridges*, John Wiley & Sons, Inc., New York.
- Scott, B.D., Park, R. and Priestley, M.J.N. (1982), "Stress-strain behavior of concrete confined by overlapping hoops at low and high strain rates", *ACI J.*, **79**(2), 13-27.
- Shim, C.S., Chung, C.H. and Kim, H.H. (2008), "Experimental evaluation of seismic performance of precast segmental bridge piers with a circular solid section", *Eng. Struct.*, **30**, 3782-3792.
- Spacone, E., Filippou, F.C. and Taucer, F.F. (1996), "Fibre beam-column model for non-linear analysis of R/C frames: Part I. Formulation", *Earthq. Eng. Struct. D.*, **25**, 711-725.
- Wang, J.C., Ou, Y.C., Chang, K.C. and Lee, G.C. (2008a), "Large-scale seismic tests of tall concrete bridge columns with precast segmental construction", *Earthq. Eng. Struct. D.*, **37**, 1449-1465.
- Wang, Z.Q., Ge, J.P. and Wei, H.Y. (2008b), "Seismic performance of precast concrete bridge column of East Sea Bridge", *J. Tongji Univ. (Natural Science)*, **36**(11), 1462-1466. (In Chinese)
- Zhu, Z.Y., Ahmad, I. and Mirmiran, A. (2006), "Fiber element modeling for seismic performance of bridge columns made of concrete-filled FRP tubes", *Eng. Struct.*, **28**, 2023-2035.

## Appendix

### A. Derivation of Eq. (11)

Assume the curvature at maximum bending moment of a cantilever column under top lateral force  $F_y$  is  $\phi_y$ , based on elastic flexure theory one can get

$$M_y = -EI\phi_y$$

where  $M_y$  is bending moment of column,  $EI$  is elastic flexural stiffness of column.

$$M_y = F_y \cdot L$$

where  $L$  is column height.

If lateral force  $F_y$  is constant for certain loading stage point, it is obvious that the curvature  $\phi_{yz}$  at certain location of column is in linear proportion with the distance  $z$  from this location to lateral force acting point.

Under constant tip lateral force  $F_y$ , the curvature  $\phi_{yz}$  at  $z$  distance from lateral force acting point can be written as

$$\phi_{yz} = \phi_y \frac{z}{L}$$

The rotation  $\theta_{yz}$  at  $z$  distance from lateral force acting point can be written as

$$\theta_{yz} = \phi_{yz} \cdot dz$$

where  $dz$  is micro length at location of  $z$  distance from lateral force acting point.

The column tip displacement  $d\Delta_{yz}$  caused by the curvature at point  $z$  and rotation in micro length  $dz$  can be written as

$$d\Delta_{yz} = \theta_{yz} \cdot z = \phi_y \frac{z^2}{L} dz$$

The column total tip displacement due to lateral force  $F_y$  can be derived by integration of above equation

$$\Delta_y = \int_0^L d\Delta_{yz} = \int_0^L \phi_y \frac{z^2}{L} dz = \frac{\phi_y L^2}{3}$$